ARTICLE IN PRESS

Solid State Electronics xxx (xxxx) xxx–xxx

Contents lists available at ScienceDirect

Solid State Electronics

journal homepage: www.elsevier.com/locate/sse

Near-field scanning microwave microscope platform based on a coaxial cavity resonator for the characterization of semiconductor structures

Bendehiba Abadlia Bagdad, Carmen Lozano, Francisco Gamiz*

Nanoelectronics Research Group, CITIC, University of Granada, 18071 Granada, Spain

A R T I C L E I N F O

Keywords:
Near-field scanning microwave microscopy (NSMM)
Coaxial cavity resonators
Non-destructive characterization
Thin film semiconductor structures

A B S T R A C T

A Near-Field Scanning Microwave Microscope (NSMM) for the characterization of semiconductor structures has been designed, simulated and fabricated. The present NSMM system is based on a home-made coaxial-cavity resonator which is fed by a Keysight N5242A PNA-X Network Analyzer. The inner conductor of the coaxial resonator is connected to a sharpened tungsten tip, which was fabricated by an electrochemical process. The reflection and transmission coefficients S_{11}, S_{21}, the resonance frequency f_r and the quality factor Q of the resonant cavity are measured as the semiconductor structure is scanned by the sharpened probe tip while the sample-tip distance is kept constant in the near-field region. The interaction between the probe tip and the sample under test provides variations of these parameters which are related to the topographical and dielectric properties of a very small region of the material under the probe tip. Thus, a 2D image of the evolution of the S_{11}, S_{21}, f_r and Q parameters on the surface of the device under test is obtained. This image can be related to space changes in the topography, dielectric properties and composition of the semiconductor structure.

1. Introduction

Near-field scanning microwave microscopy (NSMM) is a technique used for the non-destructive characterization of materials at microwave frequency range. An NSMM system consists of a sharpened metallic tip, mounted on the center conductor of a high-quality coaxial resonator. The coaxial resonator is fed by a microwave signal supplied by a Vector Network Analyzer (VNA). The transmission coefficient $S_{21,}$ (resp. reflection coefficient, S_{11}) of the cavity, measured by the VNA, shows a characteristic transmission maximum (resp. reflection minimum) at the resonant frequency, f_{r0}, for which it was designed, and a particular quality factor, Q_0, which also depends on the geometry of the cavity. When the probe tip is placed close enough (in the near field region) to the device under test (DUT), a shift in the resonant frequency f_r and a modification of the quality factor, Q, of the coaxial-cavity resonator are produced depending on the impedance of the tip-sample interaction. These changes are continuously measured by the VNA. The shift of the resonant frequency depends on the distance between the tip and the sample and the electromagnetic properties of the sample under test, such as the conductivity, sheet resistance, or dielectric constant, and their spatial variations [1–4]. If the distance between the tip and the surface of the sample is kept constant, the shift in f_r only depends on the electromagnetic properties of a very small area (of the size of the tip dimensions) of the DUT near the probe tip. The sample is then scanned by the tip of the cavity while the distance between tip-sample is kept constant and the resonant frequency of the cavity is continuously measured by the VNA. The 2D representation of the resonant frequency, f_r, quality factor Q, and magnitude of the transmission $|S_{21}|$ and reflection $|S_{11}|$ coefficients of the coaxial-cavity resonator provides a map of the electromagnetic properties of the sample under test. Therefore, the high spatial resolution of the NSMM technique allows us to non-destructively characterize semiconductor structures with high sensitivity and with nanoscale resolution without damaging them [5,6]. Thus, we can evaluate, for example, the quality of the interfaces, layer thickness variations, doping and concentrations, etc. [7].

Fig. 1 shows the scheme of the NSMM structure with the main parts of the system, such as the VNA that continuously feeds a coaxial-cavity resonator with a conductive tip connected at the end of its inner conductor.

The designed coaxial-cavity resonator provides a very high-quality factor and its potential to characterize metallic materials has been already demonstrated by several groups [7,8]. In this paper, the design, simulation and set up of a NSMM platform based on a coaxial-cavity resonator have been carried out. Then, the transmission and reflection coefficients S_{21}, S_{11} of the resonant cavity is continuously measured and monitored by a vector network analyzer, while a sharpened tungsten tip

* Corresponding author.
E-mail address: fgamiz@ugr.es (F. Gamiz).

https://doi.org/10.1016/j.sse.2019.03.052

0038-1101/ © 2019 Elsevier Ltd. All rights reserved.

Please cite this article as: Bendehiba Abadlia Bagdad, Carmen Lozano and Francisco Gamiz, Solid State Electronics, https://doi.org/10.1016/j.sse.2019.03.052

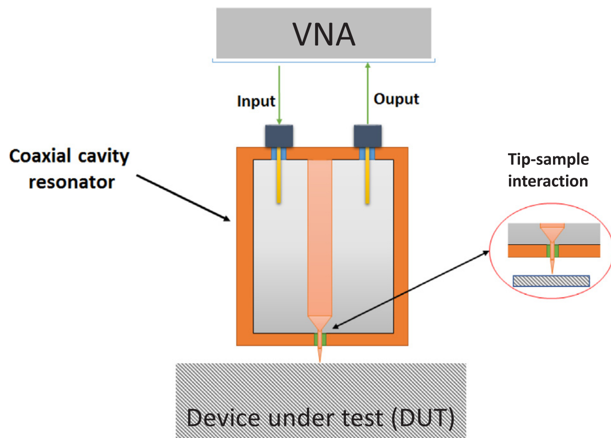

Fig. 1. General scheme of a near-field scanning microwave microscope based on a cylindrical coaxial cavity.

placed at the edge of the central conductor of the coaxial-cavity is moved over the device under test at a very short distance (near field region). We figure out that the spatial variations of the resonant frequency f_r, the maximum (resp. minimum) of $|S_{21}|$ (resp. $|S_{11}|$) and quality factor, Q, are then related to the spatial variations of the electromagnetic properties, and therefore of the composition, of the studied sample in an area whose size is of the order of magnitude of the tip thickness. This technique could then be used to non-destructively characterize semiconductors structures with micrometric or even nanometric spatial resolution [9].

2. Design and simulation

Fig. 2 shows the scheme of the NSMM resonant cavity based on an λ/4 coaxial resonator. As observed, the coaxial resonant cavity is formed by a hollow cylinder of copper with internal radius “R”, and height “h”, being “d”, the thickness of the cylinder walls. A top and a bottom copper taps close the cavity, which has an inner copper rod of diameter “b” in its axis. The lower tap presents an aperture of radius “a” which is filled with a dielectric (sapphire or Teflon). A very sharp tungsten tip is then fixed to the lower edge of the inner conductor,

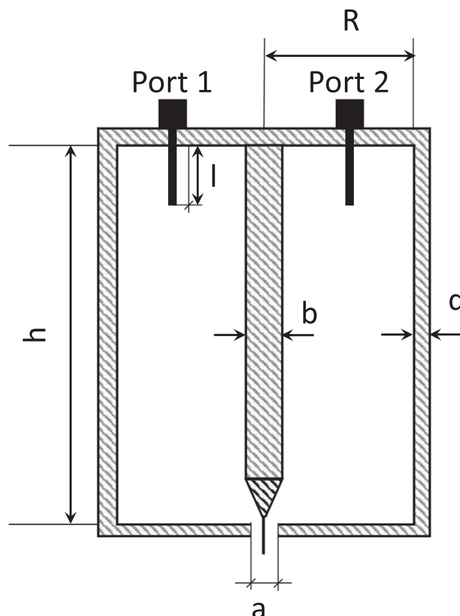

Fig. 2. Scheme of the designed coaxial cavity with the corresponding parameter definition.

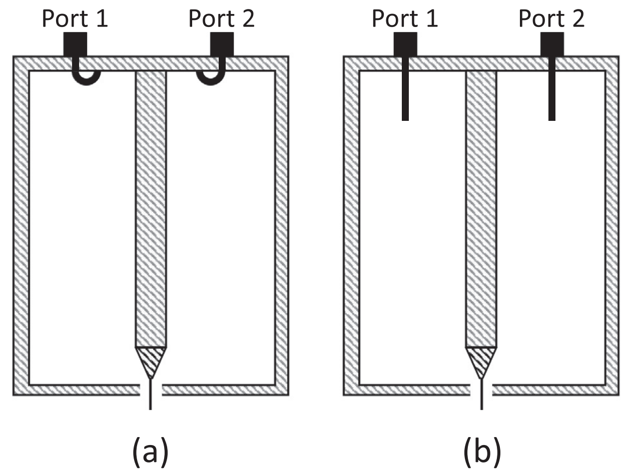

Fig. 3. Scheme of (a) the cylindrical coaxial resonant cavity excited with coupling loops (magnetic field coupling) and (b) with coupling wires (electric field coupling).

crossing the aperture and poking out some hundreds of microns of the surface of the cavity [10].

Energy has to be fed into the cavity and taken out from it to be useful as a filtering element, and to measure the properties of the device under study placed in the near-field region of the cavity tip. Excitation techniques of waveguides can be used for coupling or exciting waves in a resonator as well [11]. The first type of system which can be used to feed the cavity is coupling loops (magnetic field coupling). Coupling loops are made by stripping back the outer conductor of the coaxial transmission line which supplies power to the resonator and bending the inner conductor into a loop which is soldered to the outer conductor (Fig. 3-a). The second approach is coupling wires (electric field coupling). Coupling wires are made by stripping back the outer conductor of the coaxial transmission lines to expose the inner conductor of the cable. This is then introduced through a hole in the cavity and placed within the resonator (Fig. 3-b).

Coupling loops (magnetic coupling) provide large coupling for modes which have a circular magnetic field such as the TEM modes. The coupling is so strong that little flexibility in changing the coupling strength remains by moving the loops further in or out of the resonator. The electric field produced by coupling wires does not couple strongly to the modes of interest. However, an advantage of the coupling wires over the coupling loops is that they offer a broader range of coupling strengths. In conclusion, for the TEM modes, coupling loops provide stronger coupling and a smaller loaded quality factors whilst the coupling wires provide smaller coupling and larger loaded quality factors [11,12]. Coupling wires also provide more flexibility to change the coupling strength. Therefore, as smaller coupling is generally desired, coupling wires are preferred. In our case, we used coupling wires to excite the cavity and to extract the energy from the cavity. The length of the coupling wires is “l”. Table 1 summarizes the parameters of the selected coaxial cavity resonator:

The NSMM system has been designed and simulated using ANSYS HFSS software [13]. Fig. 4-a shows the simulated coaxial-cavity resonator designed having a cylindrical form and a closer detail of the tip connected to the inner conductor of the cavity. A tungsten tip with a final diameter of 1.5 µm is connected at the edge of the inner conductor of the coaxial cavity through the lower wall of the cylinder which forms

Table 1
Geometrical parameters of the cylindrical coaxial cavity resonator.

R	b	h	d	l
17 mm	4 mm	38.6 mm	2 mm	14 mm

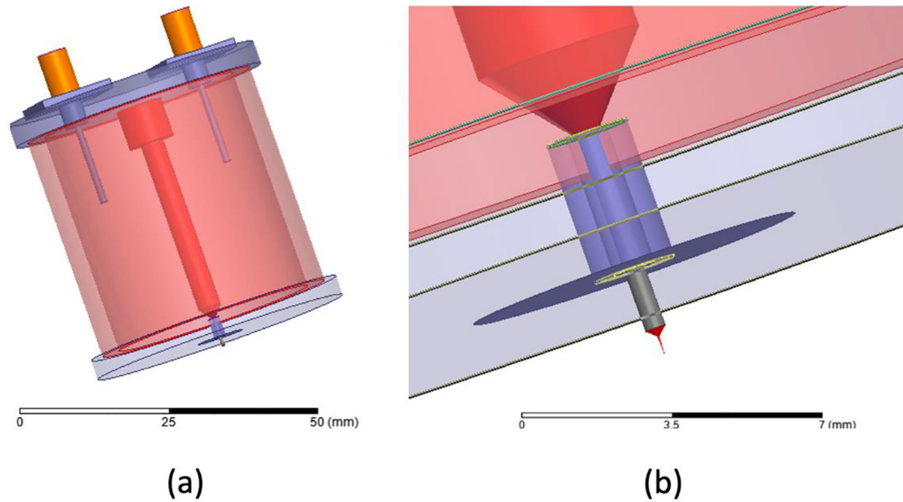

Fig. 4. Simulation in Ansys HFSS of the resonant cavity. a): Complete cavity. b): Detail of the tip.

the cavity, Fig. 4-b. The whole system is then simulated using Ansys HFSS software.

The simulated magnitude of S_{21} transmission coefficient is shown in Fig. 5 in the range 1 Mhz to 12 Ghz. No tip is connected to the edge of the inner conductor. Both magnetic coupling (Fig. 2a) and electric coupling (Fig. 2b) are considered. Several modes are activated in each case. Depending on the coupling method, some modes are less excited than others. In addition, the coupling elements also introduce extra resonant modes in the cavity that screens and modify the native cavity modes.

The strength of the coupling to the resonator can affect the sensitivity of measurements of $|S_{21}|$, and hence loss. In the case of measurements of extremely lossy samples this can be used to make the resonator less sensitive to losses so that an adequate signal to noise ratio can be maintained.

In both cases, coupling loops and coupling wires, the length of the coupling device in the cavity can be adjusted from outside the cavity. In general, the further in the cavity the coupling device is extended, the stronger the coupling. We have also studied the effect of the length of the coupling wire in the cavity. Four values of the coupling wire length were considered: l = 19 mm, 14 mm, 9 mm, and 4 mm. An arbitrary vertical axis was used in Fig. 6 so we can represent all the traces on top of one another in the same figure.

As observed, some modes do not shift in frequency with the change

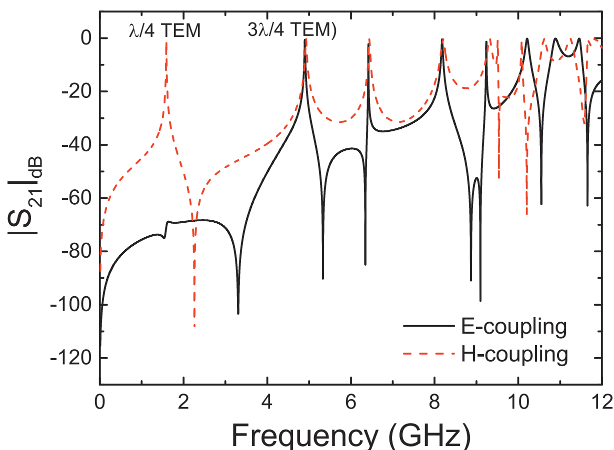

Fig. 5. $|S_{21}|_{dB}$ of the designed cavity in Table 1, calculated with ANSYS HFSS software. Both electrical coupling (l = 14 mm) and magnetic coupling is considered to feed the cavity. No tip is set at the end of the inner conductor in these results.

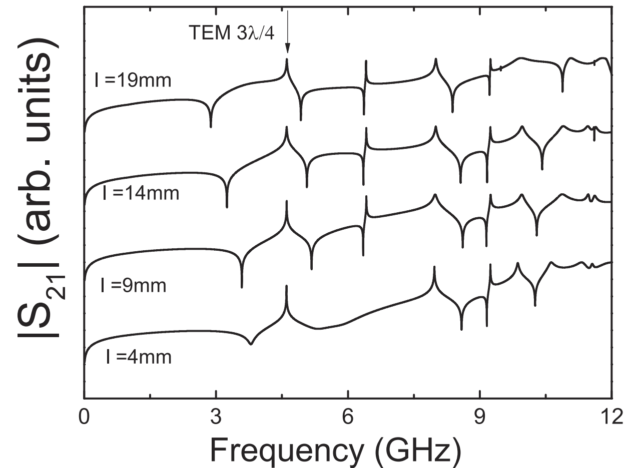

Fig. 6. $|S21|_{dB}$ (Arbitrary units) of the designed cavity for different values of the coupling wire length (E-coupling).

in the coupling wire length. This means that these modes are resonating within the cavity structure itself rather than around the coupling wires. The coupling wires protruding down into the cavity between the inner and outer conductor can emulate a coaxial structure enabling modes to resonate along the coupling wire length (coupling wire modes), instead of the cavity length (cavity modes) [14]. Hence modes which changed in frequency appreciably as the coupling wires moved into the cavity are coupling wire modes. In this way the cavity modes were differentiated and separated from coupling wire modes. The ¾ λ TEM [15] mode is one of the modes which remains constant regardless the coupling wire length, and has been selected as the working mode in the present work.

The introduction of the tip in the inner conductor of the cavity through the bottom tap also produces a drift in the resonant frequency as observed in Fig. 7. This figure compares $|S_{11}|$ and $|S_{21}|$ of the cavity without the tungsten tip, and when the tip is connected, calculated with ANSYS HFSS.

The connection of the tip reduces the resonant frequency and increases the quality factor. The tip enlarges the length of the inner conductor, and therefore the wavelength of the resonance.

In all the previous simulation results, the cavity is placed in air, far away from the sample under study (tip-in-air configuration). When the tip approaches the device under test, the resonance frequency decreases as a consequence of the interaction between the tip and the sample. Fig. 8 shows the calculated transmission coefficient of the cavity as the

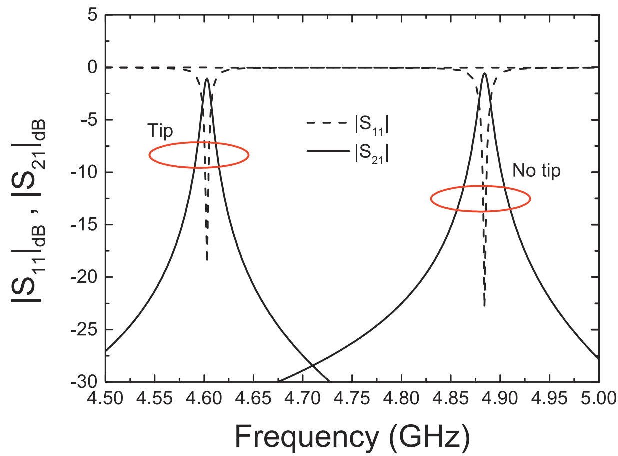

Fig. 7. Simulated $|S_{11}|_{dB}$ (dashed line) and $|S_{12}|_{dB}$ (solid line) of a coaxial cavity when the tungsten tip is placed at the edge of the inner conductor of the cavity (left) and when no tip is present (right).

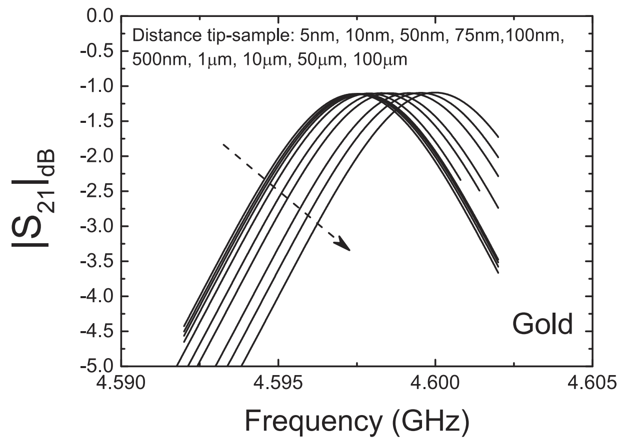

Fig. 8. Calculated $|S_{21}|_{dB}$ in the coaxial-cavity as the tip is approaching a surface of gold. The distance between the tip and the sample is reduced.

tip approaches the surface of a gold substrate:

3. Experimental setup

Once the coaxial cavity has been designed and simulated, it has been fabricated in the Micromachining Laboratory of the University of Granada. Fig. 9 shows a picture of the fabricated cavity. The coaxial cavity is shown opened; thus, the inner conductor and the coupling wires can be appreciated.

To increase the spatial resolution, a very sharp tip is set in the extreme of the inner conductor. Once the cavity is closed, a tungsten wire with a diameter of 250 μm is placed at the end of the inner conductor through the outer wall of the lower face of the cylindrical cavity, in a way that a short piece of wire (around 2 mm) pokes out from the cavity. Then, the tip is sharpened electrochemically on-site using the setup shown in Fig. 10.

Electrochemical etching has been an useful method for fabricating scanning probe microscopy (SPM) tips since the late 1980s [16]. Etching of tips occurs at the electrolyte/metal interface, and is driven by the geometry of the meniscus formed when a wire is placed into the electrolyte solution (2 N NaOH in our case) [17]. Because initial etching of the wire changes its shape, the meniscus automatically descends during the etching process, typically resulting in sharp probes [16]. The sharpening of the tip on-site, i.e., once introduced the tungsten wire through the cavity wall, allow us to allocate the sharp tip in a very short distance from the cavity, hundreds of microns, avoiding to twist or

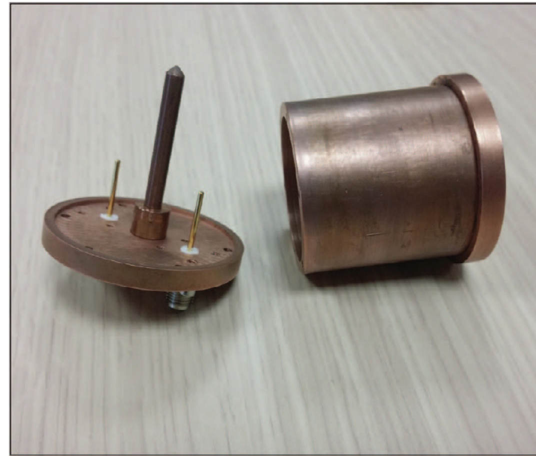

Fig. 9. Fabricated coaxial cavity resonator.

break the tip. Fig. 11 shows an optical microscope picture of the sharpened tungsten tip using the electrochemically setup shown in Fig. 10.

Once the cavity and tip have been fabricated, all the system is placed in a rack and pinion mount fixed through a vertical stainless-steel post to an optical breadboard with soborbothane feet to provide vibrational isolation. An XYZ mobile stage with micrometric resolution in XY and sub-micrometric resolution in Z (vertical) is placed on the breadboard under the cavity. The sample to be analyzed is placed on top of the mobile stage. This allows us to scan the sample in the XY plane, while the surface of the sample can be moved close to the tip down to nanometric distances. The cavity is then connected to the VNA (Keysight N5242A PNA-X Network Analyzer) and a frequency sweep is performed from 10Mhz to 26.5 GHz. Fig. 12 shows the measured broadband spectrum of $|S_{21}|$ in dB of the cavity when the tip is placed very far from the sample (air configuration).

A peak of the transmission coefficient $|S_{21}|$ appears at a frequency of $f_r = 4.6050$ GHz. At this frequency, the maximum of the $|S_{21}|$ is -11 dB and the quality factor $Q_0 = 500$. This frequency range, 4.6050 GHz, was the selected one to perform the experimental demonstration of the NSMM.

4. Results and discussion

To check the validity of the NSMM set-up, we have selected a very simple and well-known semiconductor structure. The device under test in this work consists of a silicon sample covered with 300 nm of dry SiO_2 thermally grown. Different patterns of gold and aluminum with several sizes and shapes are deposited on top of the oxide by thermal evaporation. The thickness of the gold metallization is around 40–50 nm, as measured by AFM technique (Fig. 13). These structures are used to calibrate the system.

Once the DUT is placed in the sample holder the tip is placed at a distance of 2um form the sample. Then the sample is slowly moved closer to the tip and the transmission coefficient, S_{21}, is recorded as a function of the Z position. Fig. 14 shows the magnitude of the transmission coefficient, $|S_{21}|$, for different values of the distance of the tip from the gold film.

When the tip is far from the sample, no strong near-field interactions are observed, so the resonant frequency is nearly constant. But when the sample approaches within few microns, f_r begins to drop because of the near field coupling to the sample. The resonant frequency decreases rapidly until we enter completely in the near field region, and the f_r becomes constant again, even though the tip goes closer to the surface. Fig. 15 shows the evolution of f_r as the sample is approaching the tip. Two cases are considered: the tip is approaching the gold pattern (solid

ARTICLE IN PRESS

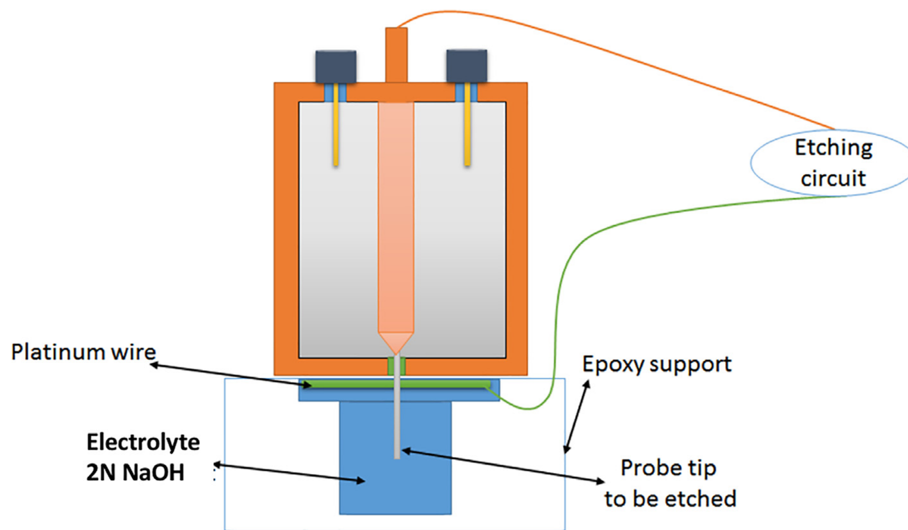

Fig. 10. Scheme of the setup used for the fabrication of the tungsten tip.

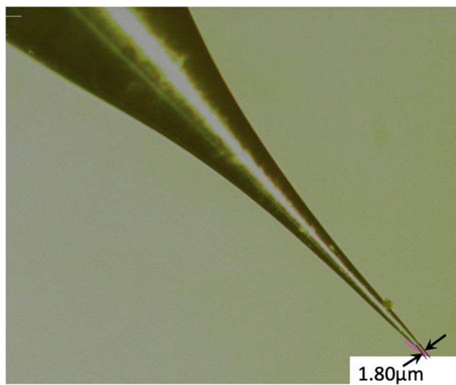

Fig. 11. Picture of the tungsten tip electrochemically sharpened. The edge of the tip has a diameter of 1.8 µm.

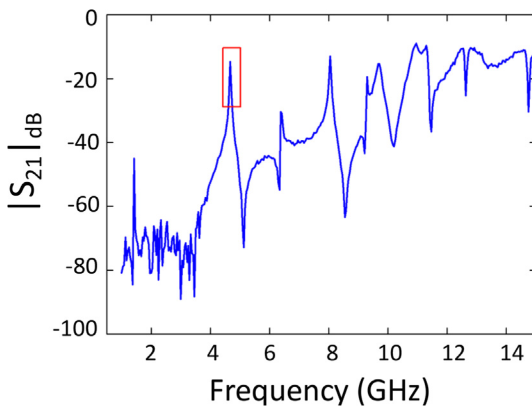

Fig. 12. $|S_{21}|$ experimentally measured in the fabricated coaxial cavity.

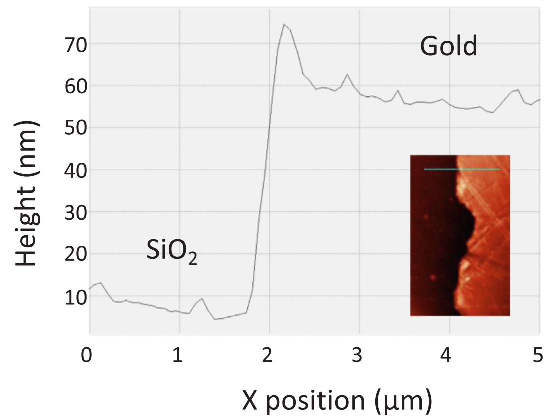

Fig. 13. AFM Profile of the gold layer deposited on top of a SiO_2/Si substrate. Gold layer thickness is around 40–50 nm (Inset: AFM 2D topography of the gold metallization).

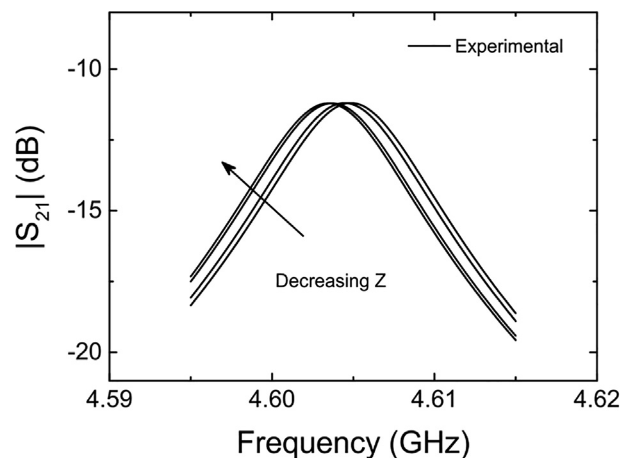

Fig. 14. Measured $|S_{21}|_{dB}$ in the coaxial-cavity as the tip is approaching the surface of the gold pattern.

line) and when the tip is moving towards the SiO_2 surface (dashed line). Z position is set to 0 at a distance around 2 µm from the sample surface.

In the first part of the curve (right side of the figure), f_r is almost constant and very similar for both SiO_2 and gold samples (Far field regime). However, as the tip moves closer to the surface of the sample, f_r decreases sharply although faster in the case of gold, and reaching lower values, thus demonstrating that the behavior of the cavity depends on the material over the one the cavity is scanned. In the approaching procedure, the Z stepper motor is stopped before the physical contact between the tip and the sample is produced, to avoid damages to the tip and/or the sample. To determine the stopping distance, the resonant frequency, f_r, as well as its first derivative, df_r/dZ are monitored continuously as a function of position, Z. In Fig. 16 the first derivative of the resonant frequency as a function of the Z is shown. Far from the surface, the derivative is zero or almost zero.

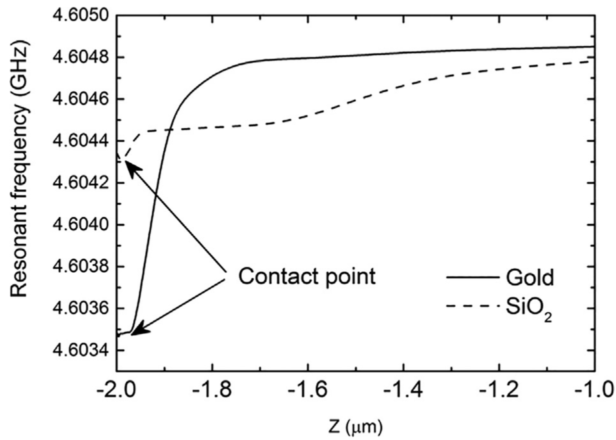

Fig. 15. Evolution of the resonant frequency as the tungsten tip is approaching the sample surface, Z.

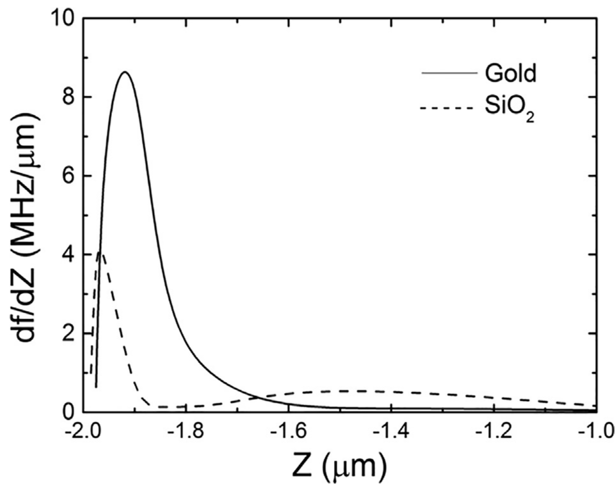

Fig. 16. First derivative of the resonant frequency, df_r/dZ versus Z position.

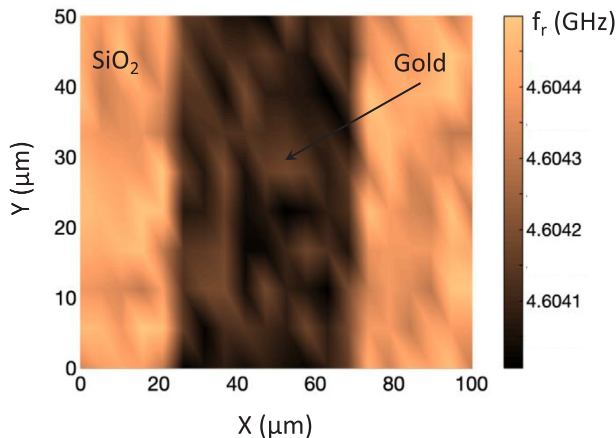

Fig. 17. 2D distribution of the resonant frequency (GHz) on a 50 μm width gold layer deposited on top of a SiO_2/Si substrate.

As the tip is approaching, and entering in the near field region, a strong increase in the derivative is produced, until a maximum is reached, followed by a sharp decrease. When the maximum in the df_r/dZ is detected, the approximation is stopped after a couple of steps, and the measurement is taken. The point where the maximum of df_r/dZ is achieved is the criterium used to consider that we are “contacting” the surface. As observed in Fig. 16, the position of the maximum of df_r/dZ is lower for the SiO2 sample than the gold sample, by approximately 50 nm. This means that the silicon dioxide surface is 50 nm below the gold surface. This is coherent with the fact that the gold layer is deposited on top of the SiO_2 layer and that according to the AFM measurements shown in Fig. 13, its thickness is around 40–50 nm. In this way, we eliminate the influence on the topography of the studied surface, and the measurement obtained only depends on the electromagnetic properties of the material under the tip. Once the maximum in df_r/dZ is reached in a given XY position, f_r, S_{21}, S_{11} and Q are measured. The tip is then lifted up to Z = 0, moved to the next scanning location in XY, and the approximation procedure is repeated in the new location. The cycle repeats until the scan over the whole DUT is complete, thus providing a 2D image of the spatial variations of the f_r, $|S_{21}|_{max}$, $|S_{11}|_{min}$, and Q. The XY spatial distribution of the Z heights where the maximum of df_r/dZ is obtained, also gives us information on the topography of the studied surface.

Fig. 17 shows the resonant frequency map of the cavity when a gold layer of 50 μm width deposited on top of a SiO_2/Si substrate is scanned. The area studied is 100×50 μm. The step increment in X and Y directions is $\Delta x = \Delta y = 5$ μm.

5. Conclusion

A near-field scanning microwave microscope (NSMM) has been designed, simulated and fabricated using a coaxial cavity resonator. A very sharp tungsten tip, electrochemically sharpened, is attached at the edge of the inner conductor of the coaxial resonator and cross through the wall of the lower face of the cavity. The resonator is feed with a Vector Network Analyzer, and the transmission coefficient $|S_{21}|$, resonant frequency, f_r, and quality factor, Q, are continuously measured, while the tip is moved close the surface of the material under study. We have demonstrated that, when the tip is placed in the near field region, the resonant frequency of the cavity depends on the electromagnetic properties of a small region of the material under it, whose dimensions are similar to the size of the tip.

Acknowledgments

The authors would like to thank the financial support of Spanish Government (TEC2014-59730-R), OTRI-UGR (Plan Propio UGR), ERASMUS MUNDUS AL-IDRISI project, and Young Researchers Program of Junta de Andalucia.

References

[1] Tabib-Azar M, Shoemaker NS, Harris S. Nondestructive characterization of materials by evanescent microwaves. Meas Sci Technol 1993;4(5):583.
[2] Bakli H, Haddadi K, Lasri T. Interferometric technique for scanning near-field microwave microscopy applications. IEEE Trans Instrum Meas 2014;63(5):1281–6.
[3] Wang YG, Reeves ME, Rachford FJ. Simultaneous imaging of dielectric properties and topography in a PbTiO 3 crystal by near-field scanning microwave microscopy. Appl Phys Lett 2000;76(22):3295–7.
[4] Steinhauer DE, Vlahacos CP, Dutta SK, Feenstra BJ, Wellstood FC, Anlage SM. Quantitative imaging of sheet resistance with a scanning near-field microwave microscope. Appl Phys Lett 1998;72(7):861–3.
[5] Melikyan H, Sargsyan T, Babajanyan A, Kim S, Kim J, Lee K, et al. Hard disk magnetic domain nano-spatial resolution imaging by using a near-field scanning microwave microscope with an AFM probe tip. J Magn Magn Mater 2009;321(16):2483–7.
[6] Wang YG, Reeves ME, Chang W, Horwitz JS, Kim W. Near-field imaging of the microwave dielectric properties of single-crystal PbTiO 3 and thin-film Sr 1? x B x TiO 3. MRS Online Proc Library Arch 1999:603.
[7] Kleismit RA, Kazimierczuk MK, Kozlowski G. Sensitivity and resolution of evanescent microwave microscope. IEEE Trans Microw Theory Tech 2006;54(2):639–47.
[8] Michalas L, Ionica I, Brinciotti E, Pirro L, Kienberger F, Cristoloveanu S, Marcelli R. Scanning microwave microscopy for non-destructive characterization of SOI wafers Vienna EUROSOI-ULIS2016. p. 238–41.
[9] Valiente LA, Haigh AD, Gibson AA, Parkinson G, Jacobs G, Withers PJ, Cooper-Holmes R. Coplanar waveguide scanning microwave profiler European Microwave ConferenceIEEE; 2007. p. 194–7.
[10] Wu Z, Souza AD, Peng B, Sun WQ, Xu SY, Ong CK. Measurement of high frequency conductivity of oxide-doped anti-ferromagnetic thin film with a near-field scanning

ARTICLE IN PRESS

microwave microscope. AIP Adv 2014;4:047114https://doi.org/10.1063/1.4871408.

[11] Chen LF, Ong CK, Neo CP, Varadan VV, Varadan VK. Microwave electronics: measurement and materials characterization. John Wiley & Sons; 2004.

[12] Pozar David M. Microwave and RF design of wireless systems. New York: Wiley; 2001.

[13] Ansys HFSS Simulation Workbench; 2018.

[14] Barker DJ. Evaluation of microwave microscopy for dielectric characterisation Ph.D. Dissertation U.K.: University of Birminghan; 2010.

[15] Marcuvitz N. Waveguide Handbook (IEEE Electromagnetic Waves Series). The Institution of Engineering and Technology; 1986.

[16] Jobbins MM, Raigoza AF, Kandel SA. Note: circuit design for direct current and alternating current electrochemical etching of scanning probe microscopy tips. Review Sci Instrum 2012;83(3):036105.

[17] Kulawik M, Nowicki M, Thielsch G, Cramer L, Rust HP, Freund HJ, et al. A double lamellae dropoff etching procedure for tungsten tips attached to tuning fork atomic force microscopy/scanning tunneling microscopy sensors. Rev Sci Instrum 2003;74(2):1027–30.